Title: Stream acidification and metal mobilization linked to permafrost degradation

Authors: Elliott K. Skierszkan[1,2*], Andras J. Szeitz[3], Matthew B.J. Lindsay[2], Sean K. Carey[3]

Affiliations:

[1]Carleton University, Department of Earth Science, 1125 Colonel By Drive, Ottawa, Ontario, Canada, K1S 5B6

[2]University of Saskatchewan, Department of Geological Sciences, 115 Geological Science Place, Saskatoon, Saskatchewan, Canada, S7N 5E2

[3]McMaster University, School of Earth, Environment & Society, 1280 Main Street West, Hamilton, Ontario, Canada, L8S 4L8

[*]Correspondence: ElliottSkierszkan@CUNET.carleton.ca

This work is a manuscript that has not been peer-reviewed and has been submitted to EarthArXiv. It is currently under review at the journal *Science*.

Abstract

We document rapid, climate-driven intensification of sulfide-mineral oxidation in permafrost-underlain headwater catchments of the Yukon and Mackenzie river basins—the two largest (sub)Arctic rivers in North America. Over the past decade, acidic (pH ~3) seepages have appeared in these headwaters that mobilize metals at acutely toxic concentrations and degrade water quality and chemistry in receiving waterbodies. These headwater processes drive multi-decadal increases in sulfate concentrations in major downstream (sub)Arctic rivers (Ogilvie, Klondike, Peel). This major perturbation in mineral weathering linked to permafrost thaw is an emergent climate–geosphere feedback with far-reaching consequences water resources, ecosystem health, and Earth's biogeochemical future.

Introduction

Large-scale degradation of water quality and enhanced global biogeochemical cycling is being driven by intensified sulfide-mineral oxidation (SMO) associated with permafrost thaw (*1*–*3*). Permafrost presently underlies >14 million km^2 of land but is currently disappearing at extents unprecedented over the Holocene Epoch (the last 11,800 years) due to post-industrial climate warming (*4*, *5*). The transition towards unfrozen ground may unlock sulfide-bearing formations that have been geochemically dormant for millennia as warming subsurface temperatures and thaw intensify interactions among water, minerals, and microbes (*2*, *6*–*16*). Sulfide minerals are globally ubiquitous in sedimentary, igneous, and metamorphic rocks, and their oxidative weathering liberates acidity, sulfate, and metals to water (*17*). SMO also indirectly modulates global climate by liberating CO_2 during acid dissolution of carbonate and silicate minerals (*18*). Runaway SMO can lead to acid-rock drainage (ARD), a condition characterized by low-pH water with elevated metal and metalloid (hereafter referred to as metals) concentrations that are toxic towards most terrestrial and aquatic organisms (*17*, *19*, *20*). SMO associated with permafrost degradation may thereby constitute a profound shift in biogeochemical cycling with global significance for water resources and aquatic ecosystems.

Significant increases in sulfate concentrations and fluxes in recent decades in the Mackenzie and Yukon river basins, which cover 2,610,000 km^2 and contribute ~20 % of discharge to the Arctic, suggest largescale SMO intensification in permafrost regions (*3*, *21*). Localized ARD onset related to permafrost thaw and deglaciation has also been observed in headwater catchments of the Spanish Pyrenees, the European Alps, and Alaskan Brooks Range, resulting in destruction of aquatic macroinvertebrate and fish communities and discoloration of streams due to mineral precipitation reactions (*1*, *22*, *23*). Understanding the breadth, timing and mechanisms of SMO acceleration in thawing permafrost requires observations linking large river basins, where solute concentrations are modulated by dilution and attenuation processes and multidecadal datasets are available, with less well-studied headwater catchments where SMO signals are most clearly manifested. Detailed hydrological and geochemical records in headwater catchments may therefore reveal the timing and mechanisms of SMO intensification not captured by the better-studied large river systems providing, for the first time, mechanistic insights into a globally significant but previously unrecognized feedback of permafrost thaw.

Here, we report abrupt onset of ARD, metal mobilization, and water-quality degradation in permafrost-underlain mountainous headwater catchments feeding the Yukon and Mackenzie river basins in the last 10 years. We studied three headwater catchments (11 to 36 km^2) in a high-latitude (~64 to 65°N) observatory, the Tombstone Waters Observatory (TWO), that straddles the Yukon-Mackenzie watershed divide in central Yukon, Canada. We linked hydrological, geochemical, and mineralogical observations in these

headwater catchments with regional remote-sensing analyses and historical water chemistry records of the major downstream rivers Peel (~74,000 km^2), Klondike (~7,800 km^2), and upper Ogilvie (~4,500 km^2) feeding Yukon or Mackenize rivers to reveal the sources and timing of SMO intensification that is affecting the Yukon and Mackenzie river basins. The nearest long-term temperature records to TWO (Dawson City, Yukon) show a 0.4°C increase per decade since 1961 (Figure S6), translating to more permafrost degradation now than at any time in the last 11,800 years (*24*). The catchments, named by their distance in kilometers from the southern limit of the Dempster Highway (KM71, KM99, and KM175), overlie pericratonic marine sedimentary rocks (limestone, shale, siltstone, sandstone, conglomerate, slate, and chert) deposited offshore of ancient North America (Laurentia). These geological terranes cover a ~867,000 km^2 area forming the Yukon/Mackenzie hydrological divide along the Yukon-Northwest Territory border (*25*). Sulfide-rich black shales capable of producing ARD are present throughout these terranes, and extend towards much of the western North American sub(Arctic) permafrost zone in Alaska, Yukon, and the Northwest Territories (*1*, *3*, *26*).

Emergent acidic seepages and accelerating sulfide-mineral oxidation reshape water quality and ecosystems along the Yukon-Mackenzie divide

We identified 130 stream reaches across ~59,500 km^2 (an area larger than Switzerland) of the Peel River basin in the TWO (upstream of the Snake River confluence) that were visibly impacted by SMO and ARD using August 2024 Sentinel-2 satellite imagery (Figure 1A). Stream discoloration extended hundreds of meters to tens of kilometers downstream of ARD inputs (Figure 1A). A large proportion of the impacted streams have relatively small catchment areas, with 49 streams draining <10 km^2, 57 streams draining 10 – 100 km^2, 27 streams draining areas 100 – 500 km^2, and three streams draining >500 km^2. Bedrock geology is a key driver of ARD, which is largely absent in carbonate-dominated catchments while it is more commonly associated with siliciclastic rocks, particularly shale and siltstone (Figure 1A). Historical (1976-2001) synoptic monitoring of headwater streams over the sedimentary terranes of eastern Yukon showed that 19 % of 10,578 sampled streams had pH <5, with acidic streams commonly associated with shale-rich headwater catchments (*26–28*). These observations affirm that vast sectors of the western North American (sub)Arctic hold geological potential to generate ARD (*26*, *28*).

Our recent (2019-2024) geochemical and hydrological monitoring of headwater streams reveals rapid and pronounced degradation of water quality because of intensified SMO, particularly since 2024. The poorest water quality in headwater streams we observed occurs in a 63 km^2 sub-catchment of the Ogilvie River that in 2000 had circumneutral pH with <100 mg L^{-1} sulfate (*27*), and has experienced considerable riparian thermokarst between 2007 and 2025 (Figure S7B and C). In July 2025, this stream had collapsed to pH 3.3, 10,800 mg L^{-1} sulfate and extreme dissolved metals concentrations including iron (670 mg L^{-1}),

aluminium (68 mg L^{-1}), zinc (33 mg L^{-1}), cadmium (13 mg L^{-1}), and nickel (11 mg L^{-1}). It produced a plume of metalliferous precipitate that was visible up to 3 km downstream of its confluence with the Ogilvie River (Figure S7A).

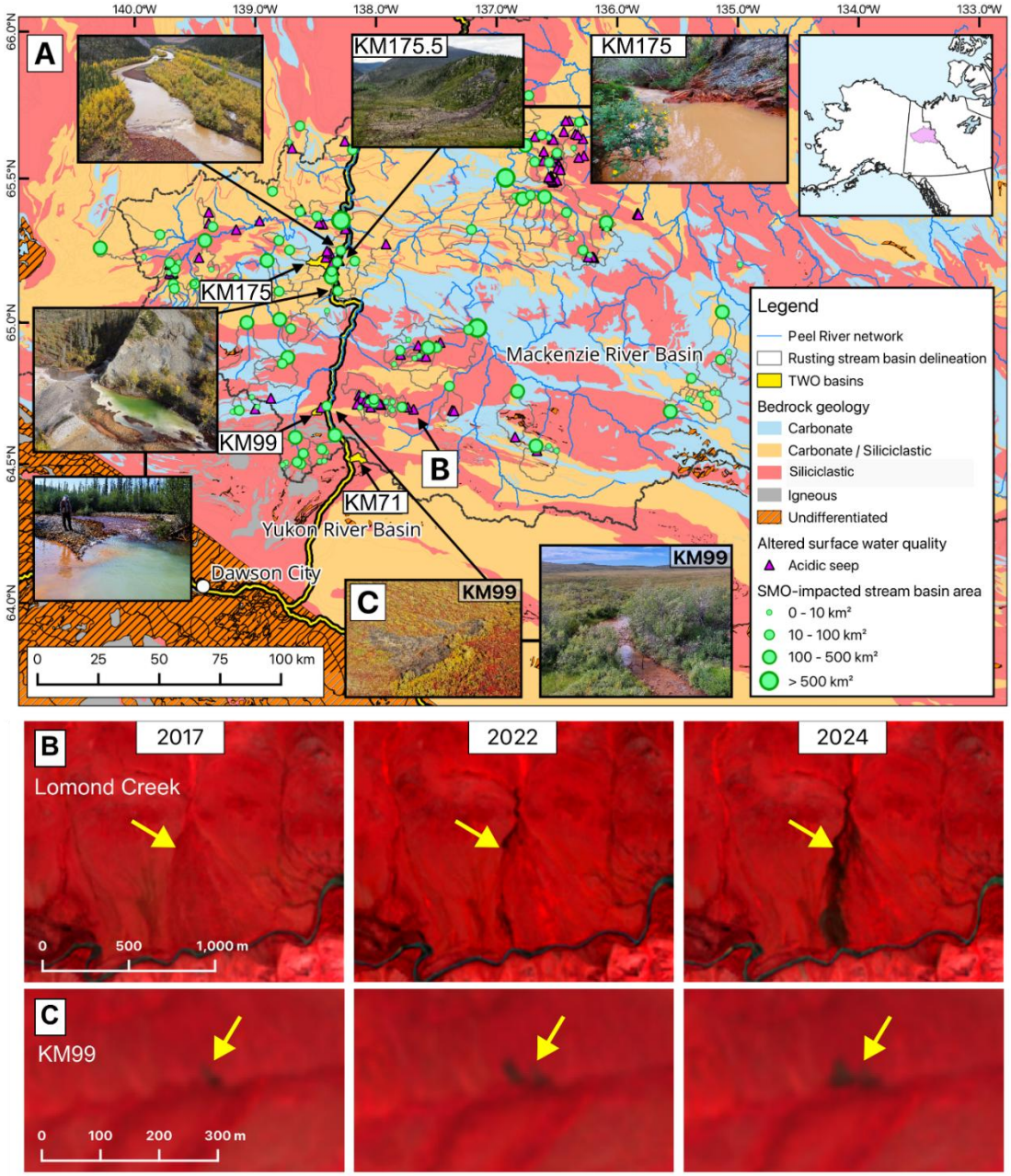

Figure 1. Regional compilation of acidic seepages, vegetation dieback, and SMO-impacted streams in the upper Klondike and Peel watersheds. *(A) Locations of SMO-impacted basins, acidic seeps, and dieback alongside simplified bedrock geology. (B) Vegetation dieback expansion over time in Lomond Creek (Hart River / Peel River catchment). (C) Vegetation dieback expansion over time in KM99 stream (in the East Blackstone River / Peel River catchment)*

In addition, field observations and remote-sensing analyses along the Yukon-Mackenzie divide within the last decade reveal pervasive vegetation dieback—patches of vegetation killed by emergent acidic seepages—up to 90,350 m^2 in area (Figure 1A, Figure 2B, Figure S8). Similar diebacks were recently reported in the Alaskan Brooks Range, suggesting this is an emergent and widespread phenomenon in the western North American (sub)Arctic (*1*). Active-layer seepages we sampled within in these diebacks in TWO also have extreme chemistry, with acidic pH (2.7–3.6), up to 17,600 mg L^{-1} sulfate, and specific conductivity of up to 13,890 µS cm^{-1} — a salinity in excess of toxicity thresholds for tundra vegetation (*29*) (Figure S8). The dissolved metals concentrations in these seepages reach up to 1,280 mg L^{-1} aluminium, 499 mg L^{-1} zinc, 138 mg L^{-1} iron, 88 mg L^{-1} manganese, 64 mg L^{-1} nickel, 6.0 mg L^{-1} cadmium, 3.7 mg L^{-1} cobalt, and 0.70 mg L^{-1} selenium (Figure S8E). These concentrations approach those at some of the world's most contaminated mine sites (*30*), surpassing toxicity thresholds for most terrestrial and aquatic organisms by several orders of magnitude and are also thousands of times above typical pristine (sub)Arctic waters (*15*, *31*, *32*). Diebacks commonly occur along or beneath hillslopes and contain oxic seepages (Figure S8), suggesting that their formation may be favored where hydraulic gradients promote infiltration of oxygenated meteoric water through expanding sulfide-bearing active-layers. Soils within vegetation diebacks harbor efflorescent sulfate mineral precipitates (gypsum, epsomite, pickeringite, tamarugite, scapolite), such that evaporative solute concentration during dry periods may contribute to vegetation stress, and could remobilize sulfate and metals during periods of intense rainfall and snowmelt (Figure S9).

The emergence of vegetation dieback is directly associated with water quality deterioration in headwater streams we have monitored in the TWO. These effects are most evident in a headwater tributary of the Peel river (KM99 stream), where a vegetation dieback first appeared circa 2015 and has grown consistently to a current size of ~1,900 m^2 (Figure 2A and Figure 1C). Active-layer seepage in the dieback area has pH of 2.7, with elevated sulfate (4,900 mg L^{-1}), zinc (499 mg L^{-1}), aluminium (303 mg L^{-1}), manganese (88 mg L^{-1}), nickel (62 mg L^{-1}), cadmium (5.1 mg L^{-1}), and other metals (Figure S8F). pH in the mainstem of the stream decreases from a value of 8.0 upstream of the dieback to 5.8 immediately downstream, where there is also an orders-of-magnitude spike in sulfate and dissolved metals concentrations (Figure S10). At the stream's confluence with the East Blackstone River, ~3 km downstream, pH rebounds towards circumneutral values (pH 6.7 ± 1.0), reflecting carbonate-dominated geology in lower stream reaches that contribute acid-buffering capacity.

Despite the small area of vegetation dieback (<0.1 % of the catchment area), inputs of ARD-impacted water drastically alter streamwater chemistry and quality until the mouth of the stream. Water downstream of the dieback was clear until 2023, when it became turbid with milky-white precipitate transitioning to

ochreous red further downstream (Figure 2C). The streambed has since been coated in white and red precipitate downstream of the seepage (Figure 2C). Interannual geochemical time-series at the mouth of KM99 stream show a recent (2023-2024) and significant decrease in pH relative to prior years (2019-2022) coinciding with an orders-of-magnitude increase in dissolved metal (cadmium, cobalt, manganese, nickel, selenium, zinc) (Figure 2A). Concentrations of these metals reach >5,000 μg L^{-1} zinc, >1,000 μg L^{-1} nickel and manganese, and >50 μg L^{-1} cobalt and cadmium, orders-of-magnitude above typical pristine (sub)Arctic streams and far surpassing environmental water-quality guidelines (WQG) set by Canada and the US Environmental Protection Agency (*33*). The rapid rate of streamwater chemistry change is captured by interannual rises in specific conductivity, with the most notable conductivity increases coinciding with the onset of visible stream discoloration in July 2023 (Figure 2C and Figure 3). This interannual specific conductivity rise overprints intra-annual variability, the latter reflecting seasonal inputs of low-specific conductivity snowmelt and rainfall during high-discharge events and more conductive deeper groundwater flowpaths during periods of low discharge (Figure 3) (*15*, *34*). Post-freshet (July-October) sulfate concentrations have been significantly higher in the stream since that time (135–221 mg L^{-1}), when compared against prior years (0.1–130 mg L^{-1}; Mann-Whitney U test $p<0.001$). Likewise, post-freshet 2024 pH (median 7.0, range 5.8–7.3) was significantly lower than prior years (median 7.6, range 7.0–8.2; Mann-Whitney U test $p<0.001$; Figure S11) and explains dissolved metal concentration increases.

Suspended particles driving streamwater discoloration are composed of metal-sulfate phases commonly associated with ARD (*35*) and sensitive to spatiotemporal evolution in streamwater pH, indicating that metal transport is modulated by complex precipitation-dissolutions along flowpaths. pH ~3 seepage dripping into the stream bank contains suspended aluminum-nickel-zinc and iron-sulfate phases with chemistry and morphology diagnostic of schwertmannite (*36*) (Figure S12E-F). Immediately downstream of this seepage and at pH 5.8, suspended particles are composed of aluminum and sulfur, typical of phases precipitating during ARD neutralization by alkaline water (*35*, *37*) (Figure S12C-D). Further downstream and at pH 7.0, suspended particles transition to aluminum and iron phases with variable sulfur, nickel, and zinc contents (Figure S12A-B). These precipitates are interpreted as nanocrystalline to amorphous aluminum hydroxides or hydroxysulfates (*38*), consistent with supersaturation with amorphous $Al(OH)_3$. Geochemical modeling suggests that conditions favorable to gypsum and jarosite precipitation occur near the pH ~3 seepage zone, while schwertmannite and basaluminite precipitation becomes more favorable downstream where pH increases from in-stream buffering (Figure S13). Ferrihydrite [$Fe(OH)_3$] precipitation is also favored at pH >6, while metal carbonates rhodochrosite [$MnCO_3$] and smithsonite [$ZnCO_3$] precipitation as pH increases above 7 (Figure S13).

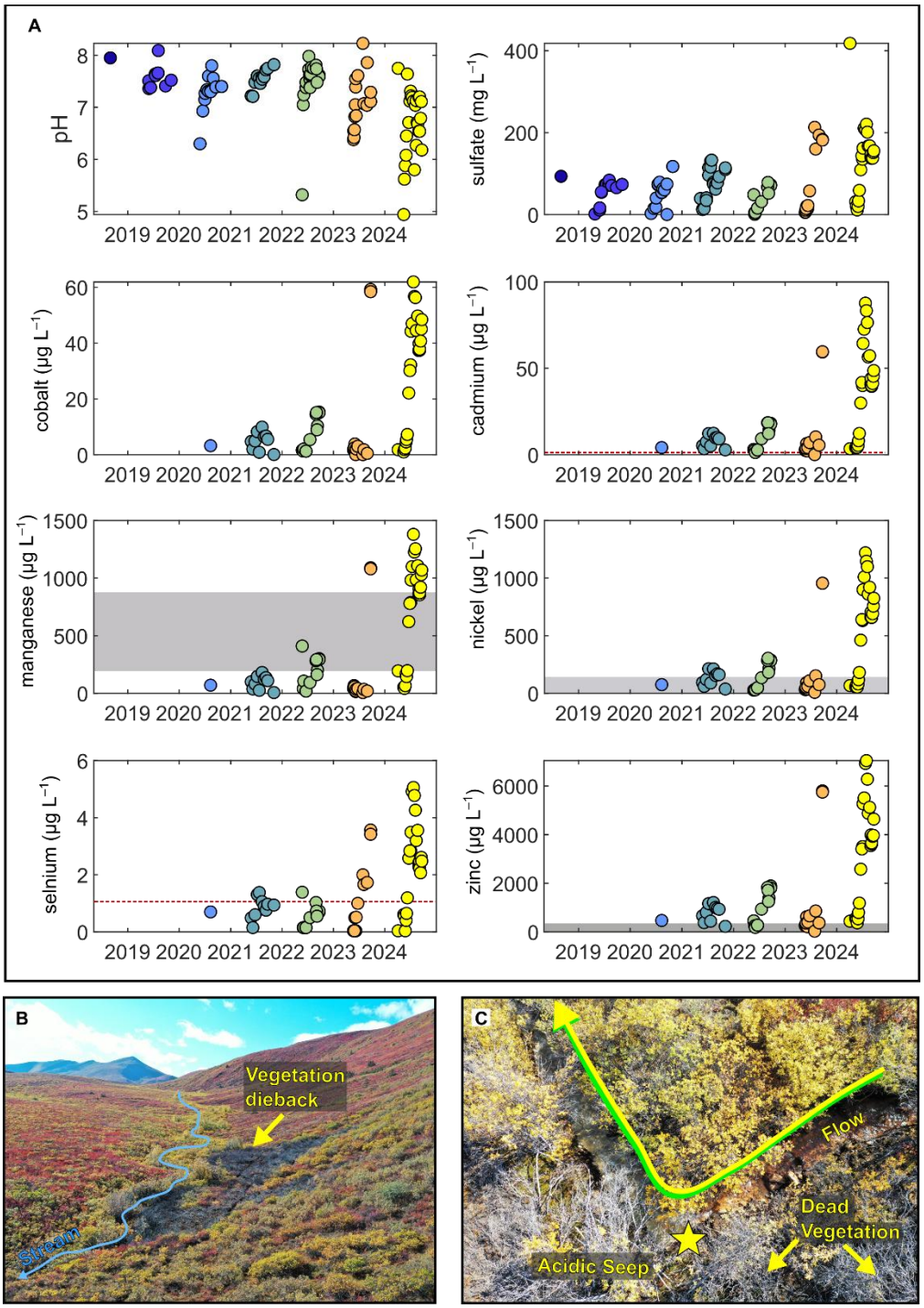

Figure 2. Recent degradation of water quality from emergent acidic seepages in headwater streams. *(A) Increasing interannual dissolved metal and sulfate concentrations and decreasing pH in a headwater stream of the Tombstone Waters Observatory (KM99 stream, Mackenzie River Basin) that has been affected by vegetation dieback (B) and discoloration (C) from incipient acidic seepage caused by sulfide-mineral oxidation. Gray shading shows the range in Canadian guidelines for the protection of aquatic life for manganese, nickel, and zinc, which vary with*

water chemistry (pH, hardness, and dissolved organic carbon content). Red dashed lines show the guidelines for the protection of aquatic life for cadmium and selenium.

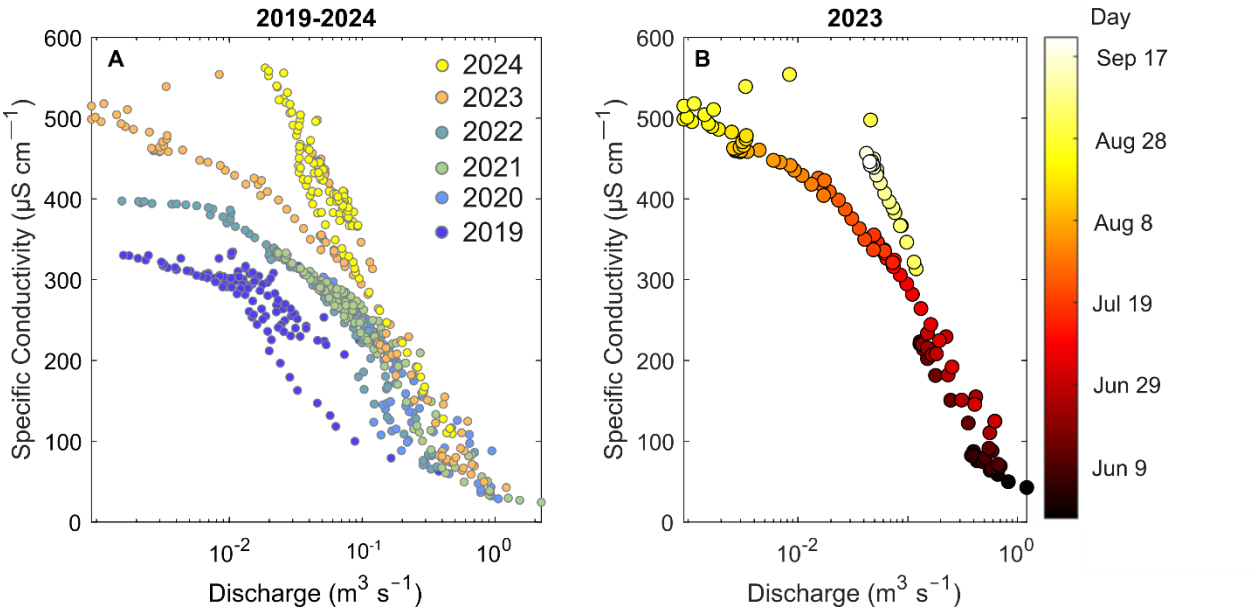

Figure 3. Rising interannual specific conductivity from intensified SMO in headwater streams. *Specific conductivity – log discharge relationships from 2019 to 2024 in a headwater stream of the Mackenzie River Basin (KM99 stream), showing a stepwise increase in specific conductivity during periods of low flow with increasing interannual conductivity over the observation period. Symbols in panel (A) are grouped by year to emphasize interannual trends. Data in panel (B) are from 2023 alone and symbology reflects day-of-year to emphasize seasonal trends.*

Widespread SMO intensification paralleling KM99 trends is also visible in other recent monitoring of headwater streams in the TWO through declining pH, increasing sulfate concentrations, and new vegetation diebacks. KM71 and KM175 streams show a similar timing of pronounced water chemistry change in 2023-2024 that includes declining pH and increasing sulfate and metals concentrations (Figure S14 and Figure S15). pH was significantly lower and sulfate significantly higher in both streams in July-October 2024 relative to prior years (Figure S11). Multiple vegetation diebacks over shale bedrock occur around KM175 stream and contain pH ~3 seepage and extreme sulfate and metals concentrations (Figure S8A, C, D). The receiving stream also shows extensive ochreous discoloration (Figure 1). These geochemical observations, coupled with the regional expansion of vegetation dieback in the last decade, point to basin-wide SMO intensification, although interannual metal trends vary among headwater catchments. KM71 and KM175 both show substantial interannual increases in dissolved cobalt, cadmium, nickel, selenium, and zinc—particularly in 2023-2024—with KM175 also exhibiting rising manganese (Figure S14 and Figure S15). As in KM99, most KM71 and KM175 water samples exceed WQG and are anomalous relative to typical pristine (sub)Arctic streams for these metals (Table S1). Variation in interannual metal trends among streams likely reflects a combination of sorption and precipitation

processes, and mixing/dilution with circumneutral to alkaline waters, which operate differently across headwaters depending on local geology and hydrological and geochemical conditions.

Rapid increases in tributary river sulfate concentrations from SMO intensification

This SMO intensification in headwater catchments along the Yukon-Mackenzie divide drives significant increases in sulfate concentrations over the last three decades in several downstream larger-order tributaries of the Yukon and Mackenzie Rivers (the Klondike, Ogilvie, and Peel Rivers) (Figure 4). Sulfate concentration time-series for the Ogilvie and Peel Rivers, which are undisturbed by local anthropogenic activity, indicate that this phenomenon arises through climate-warming driven SMO intensification. It can be assumed that similar mechanisms drive interdecadal sulfate concentrations in the Klondike River, although here additional anthropogenic disturbances cannot be ruled out because it also holds extensive placer mining operations. Additionally, the *rates* of sulfate concentration increase are rising considerably in all three rivers which suggests accelerated SMO (Figure 4). The rate of sulfate concentration increase in the Peel River, which has the most comprehensive interdecadal dataset of these rivers, has doubled between 1979-2000 and 2000-2025 to +2.1 mg L^{-1} yr^{-1}. Although the Ogilvie and Klondike River datasets have gaps between the late 1990s and the early 2000s, their rates of sulfate concentration increases during monitoring in the 2000s are +12 mg L^{-1} yr^{-1} (Ogilvie, 2016-2025) and +1.6 mg L^{-1} yr^{-1} (Klondike, 2005-2025). In contrast, these rates were marginally significant ($p=0.04$ in the Ogilvie) to non-significant ($p=0.97$ in the Klondike) during the late 1990s. These rapidly rising rates of sulfate export, particularly over the last 10 years during which we observe emergent vegetation dieback induced by ARD onset and degradation of headwater stream water quality, underscore how intensified headwater weathering processes drive nonlinear and subcontinental-scale trends of enhanced sulfate export that characterize multiple major tributaries of the Yukon and Mackenzie Rivers (*3*, *21*).

Despite these added inputs of acid derived from SMO intensification, pH remains alkaline and stable in the large downstream rivers (Klondike 7.9 ± 0.2, Ogilvie 8.1 ± 0.2, and Peel 7.9 ± 0.4), reflecting within-catchment buffering processes. Riverine dissolved and total metals (aluminum, iron, manganese, nickel, and zinc) exhibit no clear interannual trends, in contrast with sulfate (Figure S16). This decoupling of metal and sulfate trends in major rivers suggests a vast pool of metals are lost through sedimentation processes along flowpaths, likely driven by pH buffering and mineral precipitation and sorption processes analogous to those we described in ARD-impacted headwaters. Metal attenuation processes across spatial scales are further revealed through pH-driven decreases in metal/sulfate ratios from ARD-impacted headwater catchments to receiving tributaries (Figure 4D). Metal transport is therefore modulated by precipitation processes, although most of the secondary minerals we observed are metastable. Their long-term fate as a sink or source is consequently uncertain because their stability depends on uncertain future

geochemical conditions in streams, rivers, and areas of sedimentation that will influence mineral recrystallization, transformation, or dissolution processes. These findings elevate SMO from a local geomorphic process to a larger biogeochemical risk, with potential to reshape freshwater chemistry over large scale high-latitude river systems.

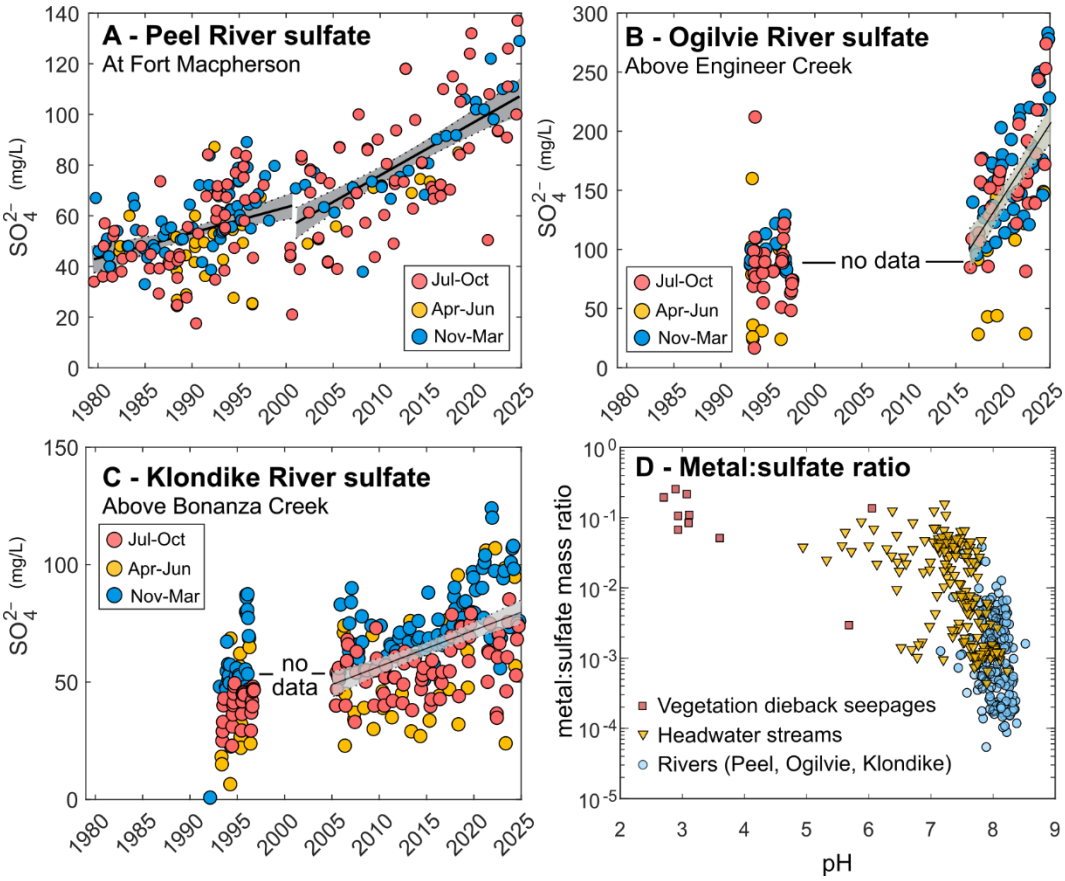

Figure 4. Recent interdecadal rises of riverine sulfate concentrations from intensified SMO in the Mackenzie and Yukon river basins. *Significant rises in sulfate concentrations have occurred in major tributary rivers of the Mackenzie and Yukon rivers downstream of the Tombstone Waters Observatory in recent decades because of intensified sulfide-mineral oxidation (A – Peel River; B – Ogilvie River; C – Klondike River). River water sulfate data symbols are grouped by season. Dissolved metal export is modulated by pH-driven precipitation and sorption processes leading to lower dissolved metals from point-source acidic seepages to receiving headwater streams and large rivers (D).*

Environmental implications of intensified sulfide-mineral oxidation in permafrost catchments

Our multiscale analysis closes a critical knowledge gap between headwater processes and multi-decadal river chemistry records (*1*, *3*, *21–23*), unveiling rapid and widespread acceleration of sulfide-mineral oxidation and associated sulfate and metal mobilization in the western North American (sub)Arctic. This phenomenon arises from the intersection of permafrost thaw with sulfide-rich sedimentary terranes—particularly black shales—that are pervasive across permafrost-underlain Alaska, Yukon, and the Northwest Territories (*1*, *26*, *28*). Our temporal geochemical records and documentation of vegetation

dieback constrain, for the first time, the timing and rapid onset of ARD within the last decade over the Yukon-Mackenzie river divide. By linking local acidic seepages to multi-decadal increases in continental river chemistry, we provide mechanistic evidence of an emergent pathway connecting permafrost thaw to global sulfur and metal cycling. This conceptual advance identifies a new Earth-system feedback with cascading consequences for aquatic ecosystems, northern communities, mineral exploration, and water-resource management.

The severity of SMO impacts depends on local buffering capacity: carbonate-rich strata can neutralize acidity but in doing so enhance CO_2 release from carbonate dissolution, adding an unexpected permafrost–climate feedback (*3*). Even under well-buffered conditions, certain hazardous metals (e.g., arsenic, antimony, nickel, selenium, uranium) remain mobile (*39*). Once initiated, acid rock drainage can persist for centuries to millennia (*40*), underscoring the long-term legacy of this process. Importantly, intensified sulfur cycling of similar magnitude accompanied the last major global climatic transition at the Pleistocene–Holocene boundary (*41*). A comparable disruption appears to be unfolding in the modern warming (sub)Arctic.

While metal transport from headwaters is partly attenuated by precipitation, sorption, and sedimentation along flowpaths, these secondary reactions do not eliminate ecological risk. Metal-rich precipitates accumulate in depositional environments, coating streambeds, stressing benthic habitats (*1*), and potentially create long-term ecological hazards as metastable precipitates recrystallize or dissolve. At larger scales, enhanced export of micronutrients such as iron and zinc (two metals characteristic of ARD and growth-limiting nutrients in the pelagic oceans (*42*)) from (sub)Arctic rivers could alter ocean productivity, even as localized acidification and metal toxicity degrade headwater ecosystems.

References

1. J. A. O'Donnell, M. P. Carey, J. C. Koch, C. Baughman, K. Hill, C. E. Zimmerman, P. F. Sullivan, R. Dial, T. Lyons, D. J. Cooper, B. A. Poulin, Metal mobilization from thawing permafrost to aquatic ecosystems is driving rusting of Arctic streams. *Communications Earth & Environment* **5**, 268 (2024).

2. E. K. Skierszkan, J. W. Dockrey, M. B. J. Lindsay, Enhanced metal mobilization from thawing permafrost is an emergent risk to water resources. *Environmental Science & Technology - Water* **5**, 20–32 (2024).

3. E. V. Walsh, R. G. Hilton, S. E. Tank, E. Amos, Temperature sensitivity of the mineral permafrost feedback at the continental scale. *Science Advances* **10**, eadq4893 (2024).

4. J. Obu, S. Westermann, A. Bartsch, N. Berdnikov, H. H. Christiansen, A. Dashtseren, R. Delaloye, B. Elberling, B. Etzelmüller, A. Kholodov, A. Khomutov, A. Kääb, M. O. Leibman, A. G. Lewkowicz, S. K. Panda, V. Romanovsky, R. G. Way, A. Westergaard-Nielsen, T. Wu, J. Yamkhin, D. Zou, Northern Hemisphere permafrost map based on TTOP modelling for 2000–2016 at 1 km^2 scale. *Earth-Science Reviews* **193**, 299–316 (2019).

5. Intergovernmental Panel on Climate Change, *Climate Change 2013 - Working Group 1 Contribution to the Fifth Assessment Report of the Intergovernmental Panel on Climate Change*, (Intergovernmental Panel on Climate Change, 2013).

6. A. J. Barker, T. D. Sullivan, W. B. Baxter, R. A. Barbato, S. Gallaher, G. E. Patton, J. P. Smith, T. A. Douglas, Iron oxidation-reduction processes in warming permafrost soils and surface waters expose a seasonally rusting Arctic watershed. *ACS Earth and Space Chemistry* **7**, 1479–1495 (2022).

7. M. S. Patzner, C. W. Mueller, M. Malusova, M. Baur, V. Nikeleit, T. Scholten, C. Hoeschen, J. M. Byrne, T. Borch, A. Kappler, C. Bryce, Iron mineral dissolution releases iron and associated organic carbon during permafrost thaw. *Nature Communications* **11**, 1–11 (2020).

8. M. S. Patzner, N. Kainz, E. Lundin, M. Barczok, C. Smith, E. Herndon, L. Kinsman-Costello, S. Fischer, D. Straub, S. Kleindienst, A. Kappler, C. Bryce, Seasonal fluctuations in iron cycling in thawing permafrost peatlands. *Environmental Science & Technology* **56**, 4620–4631 (2022).

9. E. Herndon, L. Kinsman-Costello, S. Godsey, "Biogeochemical cycling of redox-sensitive elements in permafrost-affected ecosystems" in *Biogeochemical Cycles: Ecological Drivers and Environmental Impact*, K. Donstova, Z. Balogh-Brunstad, G. Le Roux, Eds. (American Geophysical Union and John Wiley & Sons, Inc., ed. 1, 2020), pp. 254–266.

10. O. S. Pokrovsky, R. M. Manasypov, A. V. Chupakov, S. Kopysov, Element transport in the Taz River, western Siberia. *Chemical Geology* **614**, 121180 (2022).

11. O. S. Pokrovsky, R. M. Manasypov, S. V. Loiko, L. S. Shirokova, Organic and organo-mineral colloids in discontinuous permafrost zone. *Geochimica et Cosmochimica Acta* **188**, 1–20 (2016).

12. O. S. Pokrovsky, M. Bueno, R. M. Manasypov, L. S. Shirokova, J. Karlsson, D. Amouroux, Dissolved organic matter controls seasonal and spatial selenium concentration variability in thaw lakes across a permafrost gradient. *Environmental Science & Technology* **52**, 10254–10262 (2018).

13. C. R. Burn, A. Bartsch, E. Chakraborty, S. Das, R. Frauenfelder, I. Gärtner-Roer, K. G. Gisnås, T. Herring, B. J. Jones, S. V. Kokelj, E. Lathrop, J. B. Murton, D. M. Nielsen, F. Niu, C. Olson, B. H. O'Neill, S. Opfergelt, P. P. Overduin, K. Schaefer, E. A. G. Schurr, E. K. Skierszkan, S. L. Smith, S. M. Stuenzi, S. E. Tank, G. Vieira, S. Westernann, S. A. Wolfe, E. Yarmak, Developments in permafrost science and engineering in response to climate warming in circumpolar and high mountain regions, 2019-2024. *Permafrost and Periglacial Processes* **36**, 167-188 (2024).

14. E. K. Skierszkan, V. A. Schoepfer, M. D. Fellwock, M. B. J. Lindsay, Uranium speciation and mobilization in thawing permafrost. *Environmental Science & Technology* **58**, 17058–17069 (2024).

15. E. K. Skierszkan, S. K. Carey, S. I. Jackson, M. Fellwock, C. Fraser, M. B. J. Lindsay, Seasonal controls on stream metal(loid) signatures in mountainous discontinuous permafrost. *Science of the Total Environment* **908**, 167999 (2024).

16. E. K. Skierszkan, V. A. Schoepfer, M. D. Fellwock, A. Hayatifar, V. F. Bondici, J. M. Mcbeth, J. W. Dockrey, M. B. J. Lindsay, Arsenic mobilization induced by thawing permafrost. *Earth and Space Chemistry* **8**, 745–759 (2024).

17. D. W. Blowes, C. J. Ptacek, J. L. Jambor, C. G. Weisener, D. Paktunc, W. D. Gould, D. B. Johnson, *The Geochemistry of Acid Mine Drainage* (Elsevier Ltd., ed. 2, 2013).

18. M. A. Torres, N. Moosdorf, J. Hartmann, J. F. Adkins, A. J. West, Glacial weathering, sulfide oxidation, and global carbon cycle feedbacks. *Proceedings of the National Academy of Sciences U.S.A.* **114**, 8716–8721 (2017).

19. M. B. J. Lindsay, M. C. Moncur, J. G. Bain, J. L. Jambor, C. J. Ptacek, D. W. Blowes, Geochemical and mineralogical aspects of sulfide mine tailings. *Applied Geochemistry* **57**, 157–177 (2015).

20. D. K. Nordstrom, C. N. Alpers, "Geochemistry of acid mine waters" in *The Environmental Geochemistry of Mineral Deposits: Part A: Processes, Techniques, and Health Issues Part B: Case Studies and*

Research Topics, G. S. Plumlee, M. J. Logsdon, L. F. Filipek, Eds. (Society of Economic Geologists, 1997), pp. 133–160.

21. R. C. Toohey, N. M. Herman-Mercer, P. F. Schuster, E. A. Mutter, J. C. Koch, Multidecadal increases in the Yukon River Basin of chemical fluxes as indicators of changing flowpaths, groundwater, and permafrost. *Geophysical Research Letters* **43**, 12, 120–12, 130 (2016).

22. M. Zarroca, C. Roqué, R. Linares, J. G. Salminci, F. Gutiérrez, Natural acid rock drainage in alpine catchments: A side effect of climate warming. *Science of the Total Environment* **778**, 146070 (2021).

23. C. Wanner, H. Moradi, P. Ingold, M. A. Cardenas Bocanegra, R. Mercurio, G. Furrer, Rock glaciers in the Central Eastern Alps – How permafrost degradation can cause acid rock drainage, mobilization of toxic elements and formation of basaluminite. *Global and Planetary Change* **227**, 104180 (2023).

24. T. J. Porter, S. W. Schoenemann, L. J. Davies, E. J. Steig, S. Bandara, D. G. Froese, Recent summer warming in northwestern Canada exceeds the Holocene thermal maximum. *Nature Communications* **10**, 1–10 (2019).

25. M. Colpron, J. L. Nelson, D. C. Murphy, Northern Cordilleran terranes and their interactions through time. *GSA Today* **17**, 4–10 (2007).

26. Y. T. J. Kwong, G. Whitley, P. Roach, Natural acid rock drainage associated with black shale in the Yukon Territory, Canada. *Applied Geochemistry* **24**, 221–231 (2009).

27. D. Héon, Stream sediment analysis, Yukon Regional Geochemical Database, (2003); https://data.geology.gov.yk.ca/Reference/42232.

28. D. Lacelle, R. Léveillé, Acid drainage generation and associated Ca-Fe-SO_4 minerals in a periglacial environment, Eagle Plains, Northern Yukon, Canada: A potential analogue for low-temperature sulfate formation on Mars. *Planetary and Space Science* **58**, 509–521 (2010).

29. S. V. Kokelj, A. G. Lewkowicz, Salinization of permafrost terrain due to natural geomorphic disturbance, Fosheim Peninsula, Ellesmere Island. *Arctic* **52**, 372–385 (1999).

30. Z. Bao, J. Bain, S. P. Holland, D. Wilson, C. J. Ptacek, D. W. Blowes, Hydrogeochemical response of a variably saturated sulfide-bearing mine waste-rock pile to precipitation: A field-scale study in the discontinuous permafrost region of northern Canada. *Water Resources Research* **58**, e2021WR031082 (2022).

31. N. Colombo, F. Salerno, S. Gruber, M. Freppaz, M. Williams, S. Fratianni, M. Giardino, Review: Impacts of permafrost degradation on inorganic chemistry of surface fresh water. *Global and Planetary Change* **162**, 69–83 (2018).

32. M. Colombo, K. A. Brown, J. De Vera, B. A. Bergquist, K. J. Orians, Trace metal geochemistry of remote rivers in the Canadian Arctic Archipelago. *Chemical Geology* **525**, 479–491 (2019).

33. Canadian Council of Ministers of the Environment, "Canadian water quality guidelines for the protection of aquatic life: Uranium" in *Canadian Environmental Quality Guidelines* (Canadian Council of Ministers of the Environment, 1999), pp. 1–9.

34. S. E. Godsey, J. W. Kirchner, D. W. Clow, Concentration-discharge relationships affect chemostatic characteristics of US catchments. *Hydrological Processes* **23**, 1844–1864 (2009).

35. D. K. Nordstrom, Geochemical modeling of iron and aluminum precipitation during mixing and neutralization of acid mine drainage. *Minerals* **10**, 1–12 (2020).

36. V. A. Schoepfer, E. D. Burton, Schwertmannite: A review of its occurrence, formation, structure, stability and interactions with oxyanions. *Earth-Science Reviews* **221**, 103811 (2021).

37. E. K. Skierszkan, J. S. Stockwell, J. W. Dockrey, D. Weis, R. D. Beckie, K. U. Mayer, Molybdenum (Mo) stable isotopic variations as indicators of Mo attenuation in mine waste-rock drainage. *Applied Geochemistry* **87**, 71–83 (2017).

38. S. Carrero, A. Fernandez-Martinez, R. Pérez-López, J. M. Nieto, Basaluminite structure and its environmental implications. *Procedia Earth and Planetary Science* **17**, 237–240 (2017).

39. B. Vriens, E. K. Skierszkan, M. St-Arnault, K. Salzsauler, C. Aranda, K. U. Mayer, R. D. Beckie, Mobilization of metal(oid) oxyanions through circumneutral mine waste-rock drainage. *ACS Omega* **4**, 10205–10215 (2019).

40. J. S. España, E. L. Pamo, E. Santofimia, O. Aduvire, J. Reyes, D. Barettino, Acid mine drainage in the Iberian Pyrite Belt (Odiel river watershed, Huelva, SW Spain): Geochemistry, mineralogy and environmental implications. *Applied Geochemistry* **20**, 1320–1356 (2005).

41. R. E. Stevens, H. Reade, K. L. Sayle, J. A. Tripp, D. Frémondeau, A. Lister, I. Barnes, M. Germonpré, M. Street, J. B. Murton, S. H. Bottrell, D. H. James, T. F. G. Higham, Major excursions in sulfur isotopes linked to permafrost change in Eurasia during the last 50,000 years. *Nature Geoscience* https://doi.org/10.1038/s41561-025-01760-x, (2025).

42. J. Duan, R. Cloete, J. C. Loock, A. Lanzirotti, M. Newville, A. Martínez-García, D. M. Sigman, P. J. Lam, A. N. Roychoudhury, S. C. B Myneni, Biogenic-to-lithogenic handoff of particulate Zn affects the Zn cycle in the Southern Ocean. *Science* **384**, 1235–1240 (2024).

Acknowledgements

Funding:

Natural Sciences and Engineering Research Council of Canada Discovery Grant RGPIN-2020-06722 (SKC)

Natural Sciences and Engineering Research Council of Canada Discovery Grant RGPIN-2020-05172 (MBJL)

Natural Sciences and Engineering Research Council of Canada Discovery Grant RGPIN-2025-04676 (EKS)

Natural Sciences and Engineering Research Council of Canada Banting Postdoctoral Fellowship (EKS)

Natural Sciences and Engineering Research Council of Canada Canada Graduate Scholarship – Doctoral (AJS)

Global Water Futures and Global Water Futures Observatory Programs, under the Canada First Excellence Research Fund (SKC, MBJL)

Author contributions: All authors contributed to conceptualization, methodology, investigation, visualization, project administration, and writing (original draft, review & editing). Funding acquisition was performed by SKC, MBJL, and EKS. Supervision was performed by SKC and MBJL.

Additional contributions: We are grateful to Dr. Arsh Grewal, Dr. Erin Nicholls, Tyler de Jong, and David Barrett for their involvement in sample collection and efforts towards establishing the Tombstone Waters Observatory. We thank Dr. Jing Chen, Dr. Valerie Schoepfer, Stu Ferry, and Ariel Panozo-Cabrera at the University of Saskatchewan's Environmental Geochemistry Laboratory for assistance with geochemical and mineralogical analyses and sample handling. The Tombstone Waters Observatories is situated on the traditional territory of the Tr'ondëk Hwëch'in and Na-Cho Nyäk Dun First Nation.

Competing interests:

Authors declare that they have no competing interests.

Data and materials availability:

Stream water and acidic seepage chemistry data are provided in the Auxiliary Supplementary Materials. Data from the Ogilvie, Klondike, and Peel rivers were obtained from Government of Canada (Environment and Climate Change Canada) National Long-Term Water Quality Monitoring Data. https://open.canada.ca/data/en/dataset/67b44816-9764-4609-ace1-68dc1764e9ea.

Supplementary Materials for

Stream acidification and metal mobilization linked to permafrost degradation

Authors: Elliott K. Skierszkan[1,2*], Andras J. Szeitz[3], Matthew B.J. Lindsay[2], Sean K. Carey[3]

Affiliations:

[1]Department of Earth Science, Carleton University; Ottawa, K1S 5B6, Canada,

[2]Department of Geological Sciences, University of Saskatchewan; Saskatoon, S7N 5E2, Canada

[3]School of Earth, Environment & Society, McMaster University; Hamilton, L8S 4L8, Canada

*Corresponding author. ElliottSkierszkan@CUNET.carleton.ca

The PDF file includes:

S.1 Methods

Description of study area

Our observations were obtained from three pristine mountainous headwater catchments that overlie discontinuous to continuous permafrost in the Tombstone Waters Observatory (TWO) and which drain into the Yukon and Mackenzie Rivers. The TWO was established in 2018 to understand impacts of climate change on high-latitude headwater catchments having minimal direct anthropogenic disturbance (Figure S5). Local bedrock is composed of Neoproterozoic to Triassic marine siliciclastic and carbonate rocks deposited along the western margin of the North American craton (Figure S5). Catchments are named by the travel distance in km relative to the southern limit of the Dempster Highway. KM71 (Black Shale Creek) is dominated by marine siliciclastic rocks including slate, shale, siltstone and sandstone and feeds the Klondike River within the Yukon River Basin, for which monthly water chemistry data records are available since 1992. KM99 (Slavin Creek) and KM175 similarly include siliciclastic rocks (shale, siltstone, sandstone, conglomerate, and chert), along with variable amounts of carbonates. KM99 and KM175 feed the Mackenzie River Basin via its tributary Ogilvie and Peel Rivers, for which monthly water chemistry data from federal monitoring programs are available since 1979 (*43*). Historical regional synoptic monitoring of headwater streams in the 1970s by the Geological Survey of Canada showed generally circumneutral pH, except for localized acidic tributaries associated with weathering of sulfidic black shales (Figure S5) (*26*, *27*).

Hydrological and geochemical monitoring

In 2018, TWO streams were instrumented with hydrometric stations equipped with staff gauges, pressure-temperature transducers (Solinst Levelogger), and specific conductivity loggers (Onset HOBO U24) near their outlets to obtain continuous measurements over the open-water period, typically from April or May to October. Field measurements of stream stage and discharge were made approximately bi-weekly during the open-water period. Site-specific rating curves were developed to derive continuous discharge from stream stage and pressure-transducer measurements. Mean daily values of discharge and specific conductivity (SpC) were computed from continuous records. Stream samples for major ion, pH, and SpC analyses were collected approximately biweekly during the open-water period, with trace-metal sampling initiated in 2021. Stream sampling coincided with manual measurements of staff gauges and stream discharge using a flow meter or salt-dilution gauging, depending on stream conditions. Field measurements of pH, specific conductivity, temperature, and dissolved oxygen were made alongside sampling events using calibrated multiparameter sondes (YSI Pro-DSS, YSI Pro Plus). The field measurements of temperature and SpC were used to drift-correct continuously operating in-stream sondes during site visits. Water samples for analysis of major anions and cations and major and trace elements

were field syringe filtered using 0.45 µm PTFE membranes and stored in acid-washed HDPE bottles or glass vials. The major and trace element samples were acidified to pH <2 using trace-metal grade HNO_3, and all samples were packed in coolers under ice for shipping to laboratories, where they were refrigerated until analyses. The same sampling protocols were applied in active-layer seepages of vegetation dieback areas, which were sampled by manually excavating a pit to the top of the permafrost and collecting and filtering the water in the field.

Geochemical analyses

Anion concentrations were quantified by ion chromatography (IC) at the University of Waterloo and the Analytical Geochemistry Laboratory (AGL) at the University of Saskatchewan. Major cation concentrations were quantified by IC at the University of Waterloo from 2018 to 2021, while major element and trace metal(loid) concentrations were quantified by triple quadrupole-inductively coupled plasma-mass spectrometry (QQQ-ICP-MS) at the AGL (Thermo Fisher Scientific iCAP TQe). The QQQ-ICP-MS was calibrated using certified standards, and an internal standard (Sc, Ge, Y, Rh, In, Tb, Ir) was used to correct for instrument drift and sample-matrix effects. Accuracy was typically better than 10 % as verified by analysis of a certified reference material (NIST1643f, National Institute of Standards and Technology). Analyses of field-filtered and field-acidified ultrapure water (>18.2 mega-ohm) confirmed negligible trace-metal contamination. Total alkalinity was measured on filtered samples by titration with H_2SO_4 to the bromocresol green-methyl red endpoint. Metals concentrations were compared against Canadian guidelines for the protection of aquatic life (long-term exposure), considering the toxicity-modifying factors (e.g., pH, DOC, hardness) as established in the guidelines.

Mineralogical analyses of precipitates around acidic seepages

Mineralogical controls on metal transport were evaluated on a subset of 2024 water samples from KM99 stream, where enhanced ARD was most pronounced, using a combination of geochemical modeling and mineralogical analyses of suspended particles. Mineralogical analyses were performed using field emission-scanning electron microscopy-energy dispersive X-ray spectroscopy (FE-SEM-EDS) at the University of Saskatchewan (Hitachi SU8010). FE-SEM-EDS analyses were performed on particles isolated from 0.45 µm syringe filter membranes. The filters were air-dried and particles were transferred onto two-sided C tape affixed to Al stubs, before coating samples in Au and performing analyses using a 14 kV accelerating potential.

Mineral identification of efflorescent precipitates forming in areas of vegetation dieback was performed using X-ray diffraction (Empyrean X-ray diffractometer, PANAnalytical) at Carleton University, Ottawa, Canada. Samples were finely ground with a mortar and pestle and mounted onto glass slides. Samples were analyzed from 10 to 90° (2θ) at a 0.02° step size and using a copper Kα X-ray source. Minerals were

identified by matching diffractogram peaks to single-phase minerals in the Inorganic Crystal Structure Database in X'Pert HighScore Plus (PW3212) software.

Geochemical modeling

Geochemical models used PHREEQC software and the PRODATA thermodynamic database (*44*, *45*), to which we also added thermodynamic data for schwertmannite (*35*). Sample equilibration with atmospheric oxygen was assumed in geochemical models to fix redox potential, which is warranted given the well-mixed and oxygenated nature of the studied streams.

Remote sensing

Vegetation dieback from acidic seepages

The extent of vegetation dieback killed by acidic seepages in KM99 stream was determined through unmanned aerial vehicle (UAV) photogrammetry in August 2024, and from Sentinel-2 (S2) L2A surface reflectance satellite imagery obtained from the European Space Agency Copernicus open data browser (accessible at https://browser.dataspace.copernicus.eu), and for a prominent example on a headwater stream of the Peel River (Lomond Creek). The drone imagery from KM99 was processed with ImageJ imagery analysis software (*46*) to compute the areal extent of the dead vegetation at KM99 as of 3 September 2024. The areal extent of the acid-killed vegetation at the Lomond Creek site was manually delineated using S2 imagery from 7 August 2024 using QGIS software. Annual S2 imagery, with nearest neighbour upsampling from the native 10 m spatial resolution of S2 to an approximate spatial resolution of 4 m, was obtained for both sites for July or August from 2016 through 2024 to determine annual changes in the areal extent of the dead vegetation.

The normalized difference vegetation index (NDVI), computed using the near-infrared (B8) and red (B4) S2 bands, was used to differentiate between un-impacted and acid-killed vegetation. The areal extents in 2024 determined at KM99 and Lomond Creek through UAV photogrammetry and manual delineation, respectively, were used to identify threshold values of NDVI in the respective 2024 S2 NDVI images which, when used to identify pixels representing dead vegetation in the acid seep, resulted in cumulative pixel areas equivalent to the delineated extents. The NDVI thresholds, which were 0.617 at KM99 and 0.593 at Lomond Creek, were applied to the annual NDVI images and differences in pixel area were attributed to changes in the extent of the acid-killed vegetation (*47*). Manual delineation using QGIS was required to estimate the dieback extent at KM99 in 2016 and 2019 due to suboptimal imagery. The estimated dieback extent was regressed against image date, with the regression slope representing the estimated dieback area growth rate.

SMO-impacted surface waters

SMO-impacted streams were identified through visual inspection of the true color composite of Sentinel-2 (S2, Copernicus Sentinel Data [2024]) satellite imagery from 5 – 7 August 2024 of the Peel River catchment to the confluence of the Peel and Snake Rivers. Streams were assessed as SMO-impacted if they displayed the characteristic rusty orange color observed in known SMO-impacted streams, such as Engineer Creek and the stream at KM99, which were used as references when assessing the S2 imagery. Catchment drainage area was manually delineated to the downstream visible extent of each SMO-impacted stream reach, typically coinciding with a confluence but occasionally attributed to suspected dilution due to flow accumulation.

S.4 Supplementary Figures and Tables

Table S1. Summary of metals and sulfate concentrations in selected Tombstone Waters Observatory streams and percentage of samples exceeding Canadian environmental guidelines for the protection of aquatic life (2019-2024 data)

	KM 99					*KM 71*					*KM 175*				
element	n	median	min	max	% exceed	n	median	min	max	% exceed	n	median	min	max	% exceed
Al	62	135	13.3	647	**56**	57	99	8.7	1,470	**49**	49	59	0.4	1,970	**43**
Co	62	6	<0.1	62	5	57	7.1	0.9	13	2	50	20	<0.1	63	0
Cu	62	0.6	<0.4	21	**15**	57	0.8	<0.4	25.0	4	50	0.3	0	2.9	2
Ni	62	153	8	1,220	90	57	43	13	105	0	50	224	1	672	**62**
Fe	51	195	24.5	897	0	47	63	4	219	0	41	2,430	22	16,800	**74**
Cd	62	9.5	<0.4	88.0	**98**	57	1.2	0.3	3	**92**	50	1.9	0.1	8.3	**100**
Se	62	0.9	<0.04	5.1	**45**	57	5.20	0	8.7	**88**	50	3.1	0.2	4.6	**94**
Zn	51	934	29	7,046	**98**	47	100	12	425	**57**	48	477	18	2,330	**100**
Mn	60	129	1	1,380	**27**	54	328	110	943	15	50	352	0.9	1,040	16
Sulfate	111	73	<0.2	418	N/A	77	591	120	1,060	N/A	70	324	8	733	N/A

Notes

"% exceed" refers to the percentage of samples exceeding Canadian Council of Ministers of the Environment (CCME) guidelines for the protection of aquatic life.

Colored highlights are used to emphasize metals with a high proportion of samples exceeding guidelines

Red => 85 % exceedence

Yellow = 50 to 85 % exceedence

Green = 10 to 49 % exceedence

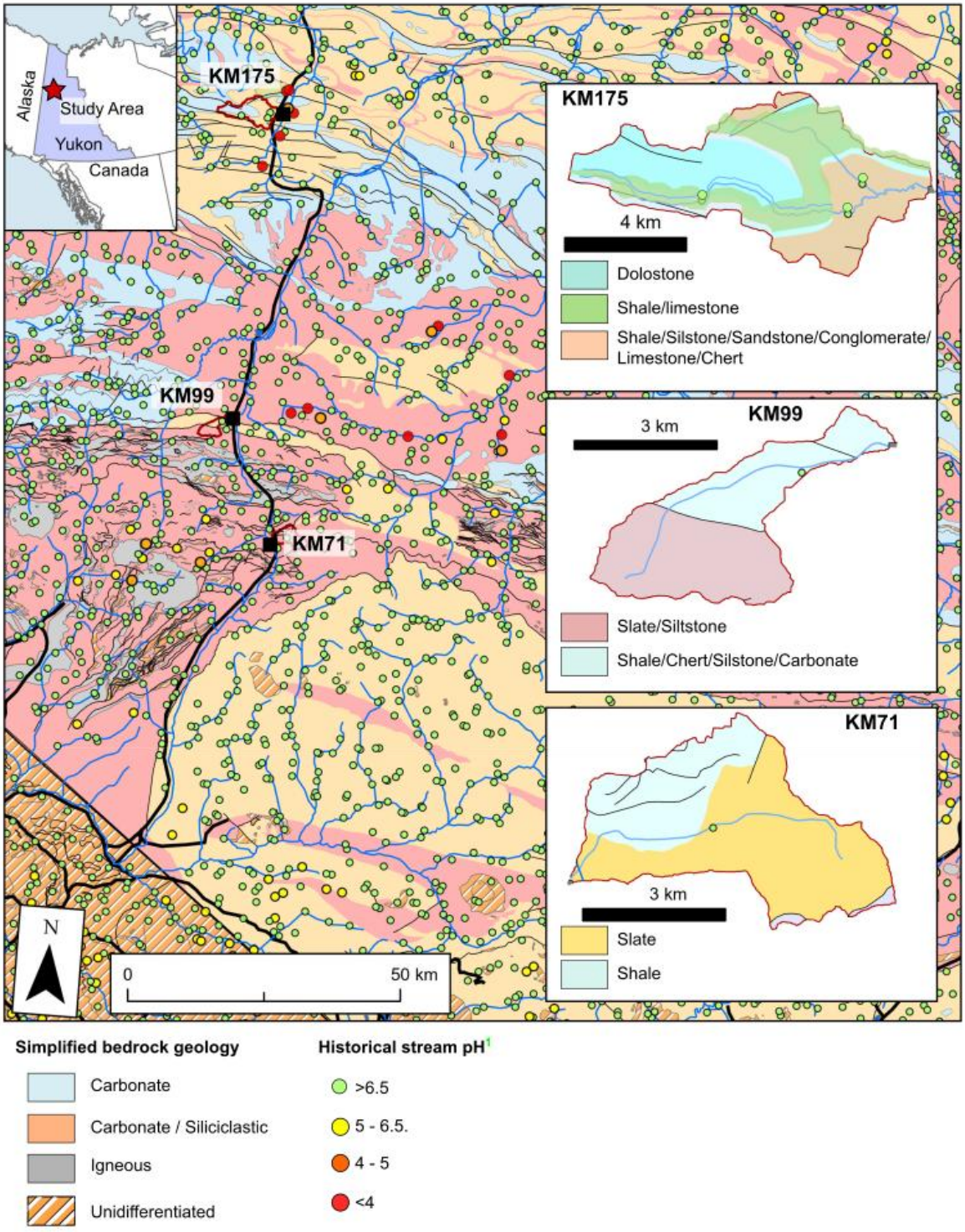

Figure S5. Study area map showing simplified regional geology and historical regional stream pH observations (27). Inset maps show catchment areas and bedrock geology in the streams studied here, and location of the Tombstone Waters Observatory within Yukon Territory, Canada.

5

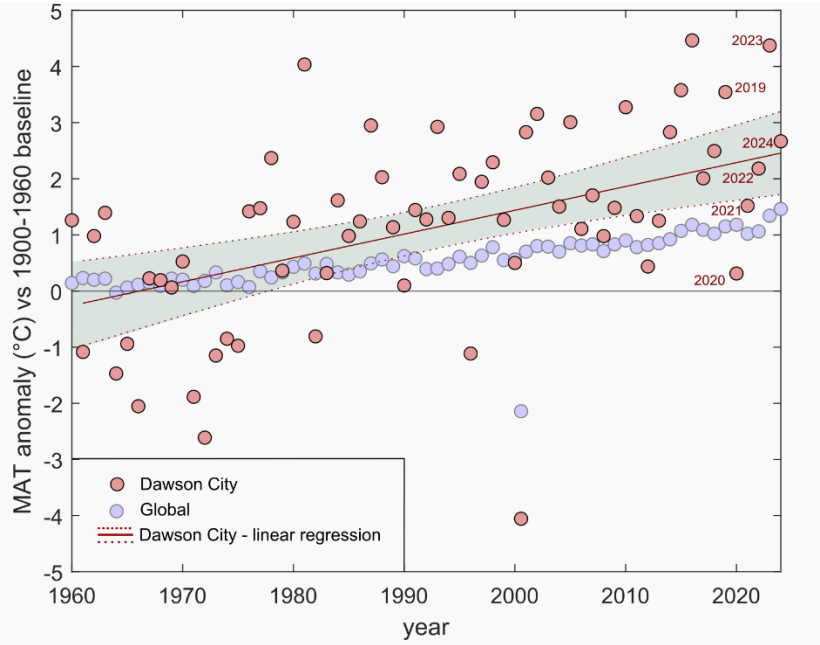

Figure S6. Mean annual temperature anomaly records for Dawson City (red circles) and global average, against a 1900-1960 baseline period. The linear regression for Dawson City temperatures shows an increase of 0.04°C yr^{-1} ($p<0.001$).

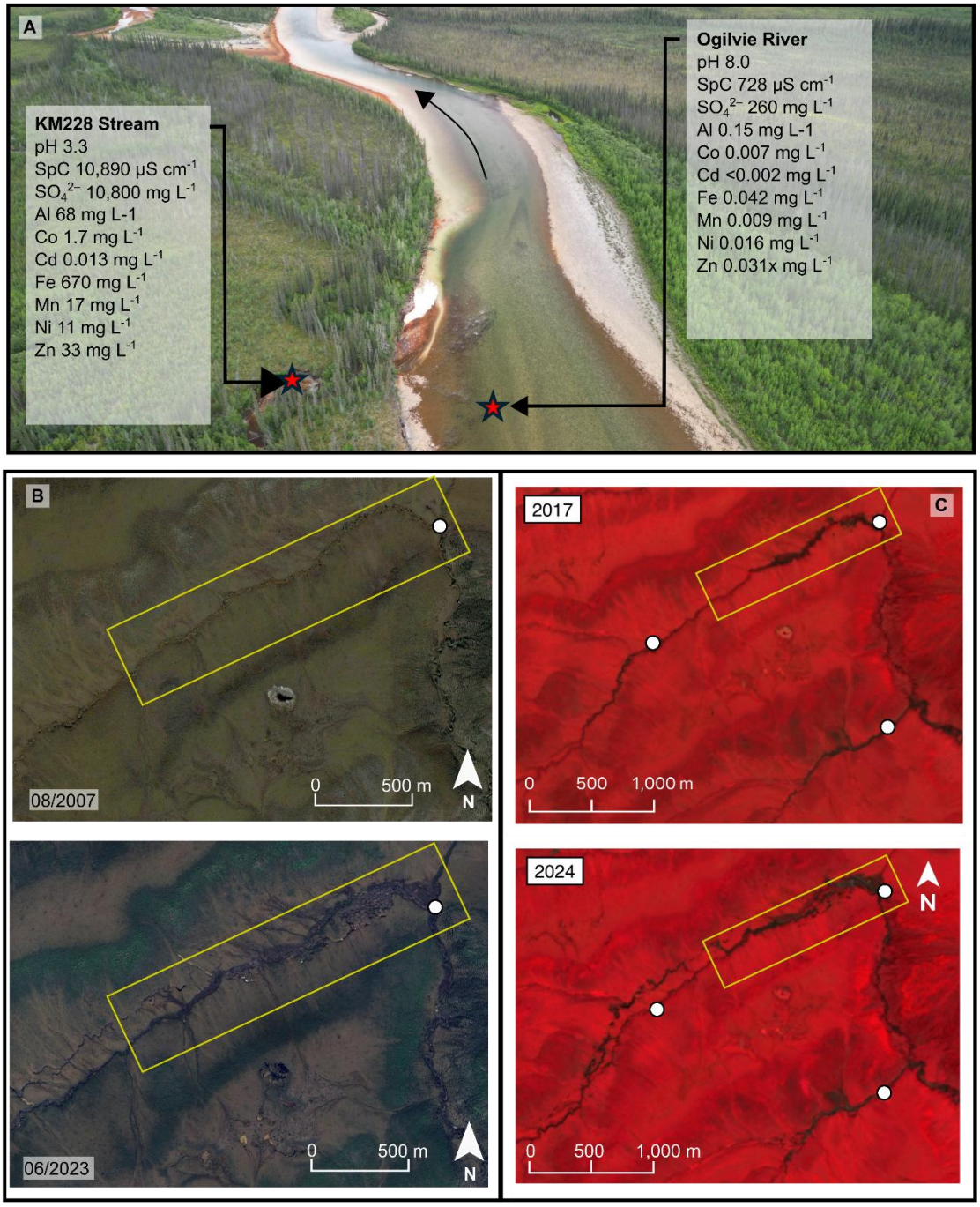

Figure S7. Acidification of KM228 stream in the Ogilvie Basin following extensive thermokarst development. (A) KM228 stream and Ogilvie River geochemical composition, in July 2025, along with the plume of metalliferous precipitate forming below their confluence. (B) Satellite imagery from 2017 and 2023 showing extensive thermokarst along the stream bank. (C) False-color composite satellite imagery of KM228 stream also showing thermokarst activity between 2017 and 2024. White circles in panels B and C indicate tributaries that were sampled in 2000 and contained circumneutral pH with <100 mg L^{-1} sulfate (27). Satellite imagery in Panel B is from Google Earth (08/2007, Maxar Technologies and Airbus) www.earth.google.com [July 24, 2025]; False-color satellite imagery in panel C is from Copernicus (Sentinel-2).

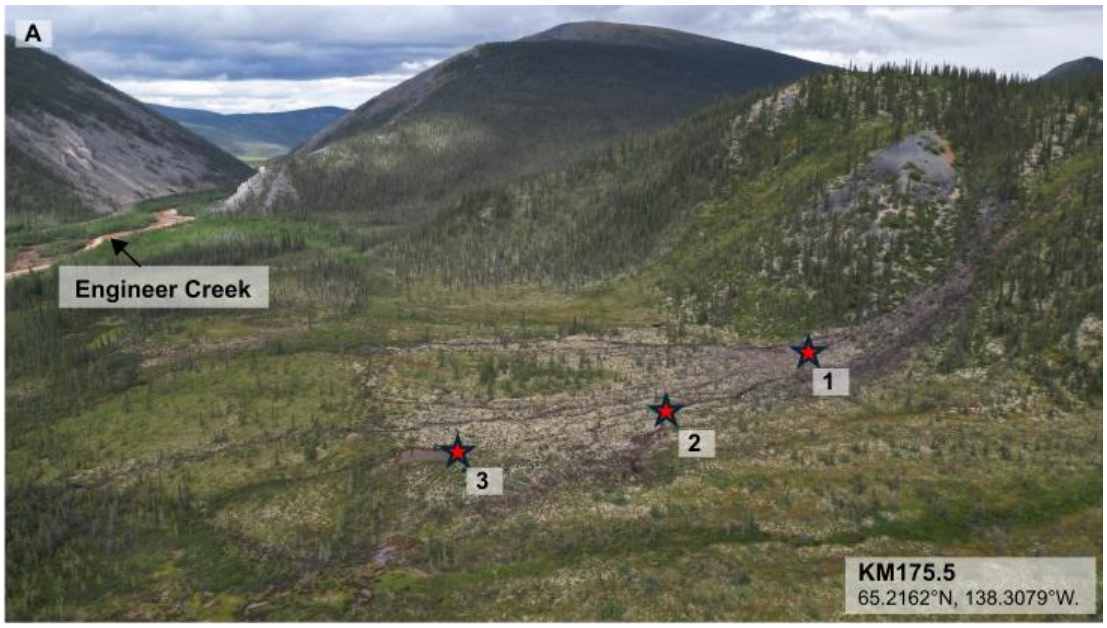

F

Location	Description	pH	SpC (µS cm^{-1})	SO_4^{2-} (mg L^{-1})	Al (mg L^{-1})	Co (mg L^{-1})	Cd (mg L^{-1})	Fe (mg L^{-1})	Mn (mg L^{-1})	Ni (mg L^{-1})	Se (mg L^{-1})	Zn (mg L^{-1})
1	Active-layer seepage	6.1	2,500	4,836	255	1.1	0.3	318	12	12	0.0090	60
2	Active-layer seepage	3.1	7,713	7,742	761	0.84	0.029	56	12	7.4	0.17	9.4
3	Upwelling Fe-stained groundwater spring	2.9	7,710	8,130	758	0.77	0.029	74	11	6.6	0.27	9.0
4	Standing Fe-stained pond	2.9	7,107	4,164	194	0.34	0.0020	76	5.4	2.9	0.70	2.1
5	Standing pond with milky-white precipitate	5.7	562	470	0.342	0.016	0.0060	0.065	0.42	0.19	0.041	0.38
6	Active-layer seepage	3.6	1,415	832	35	0.066	0.011	4.1	2.0	0.3	0.085	0.69
7	Active-layer seepage	3.1	13,890	17,610	1,277	1.8	0.1	44	28	36	0.62	92
8	Active-layer seepage	2.7	4,263	4,924	303	3.7	5.1	2.8	88	62	0.12	499
8	Seepage entering stream bank	3.1	2,001	1,179	59	0.001	1.5	56	18	15	0.038	107
8	Seepage entering stream bank	2.9	5,440	4,710	298	0.003	6.0	286	67	64	0.15	484

Figure S8. Emergent acidic seepages and vegetation dieback in headwater catchments of the Mackenzie and Yukon river basins Aerial images (A-D) are from 2025 and (E) from 2024. Chemical analyses are from 2024-2025.

Figure S9. Efflorescent white precipitates forming in areas of vegetation dieback and composed of sulfate mineral precipitates epsomite, gypsum, pickeringite, and scapolite identified by X-ray diffraction.

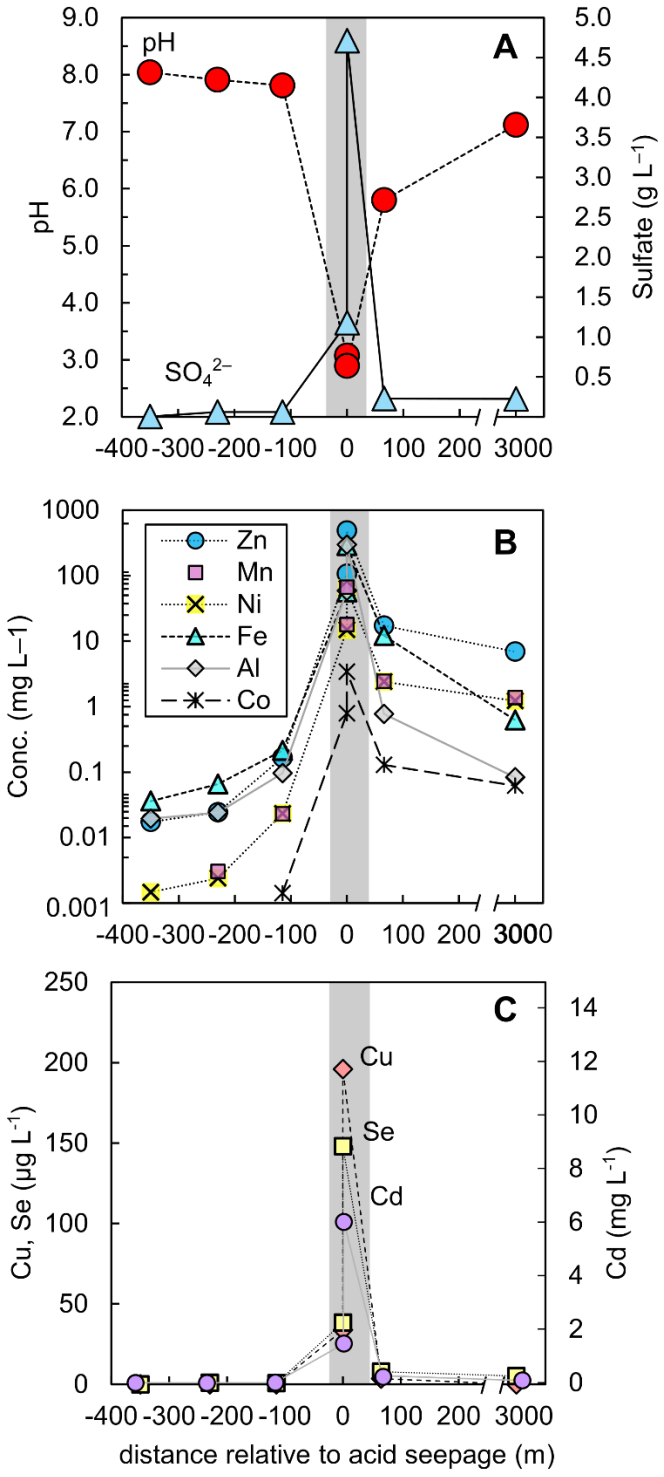

Figure S10. Spatial evolution of KM99 stream water pH and sulfate (A) and dissolved metals (B) and (C) in the vicinity of acidic seepages in KM99 in July/August 2024. Gray shading highlights area of acidic seepage adjacent to the stream.

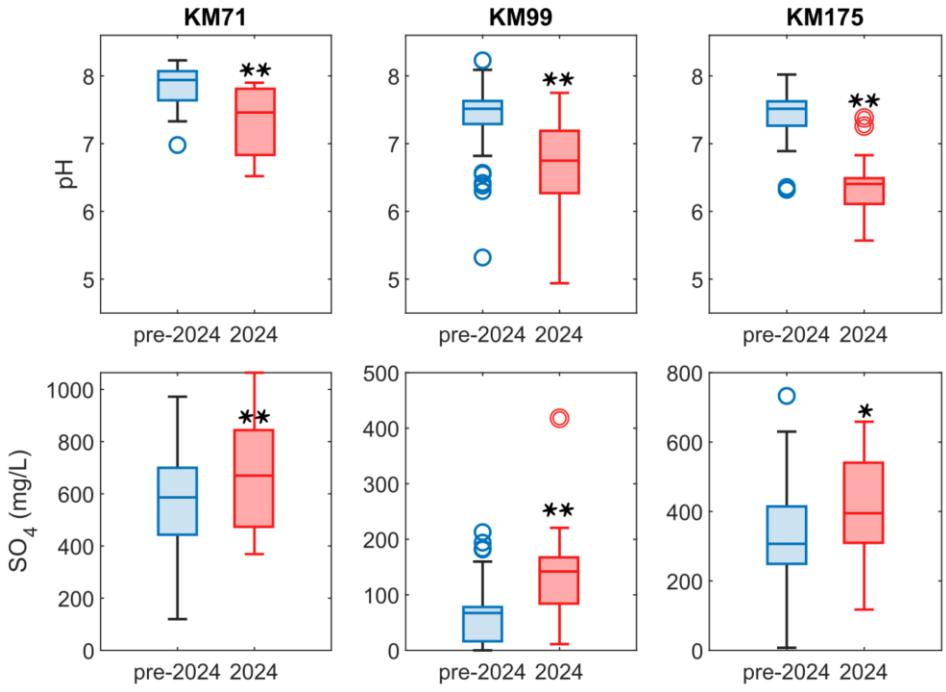

*Figure S11. Significant decreases in pH and increases in sulfate are visible in headwater streams of the Tombstone Waters Observatory in post freshet (July-October) 2024 relative prior years (2019-2023). Asterisks denote statistical significance as assessed by Mann-Whitney U test: * = p<0.05, ** = p<0.001.*

5

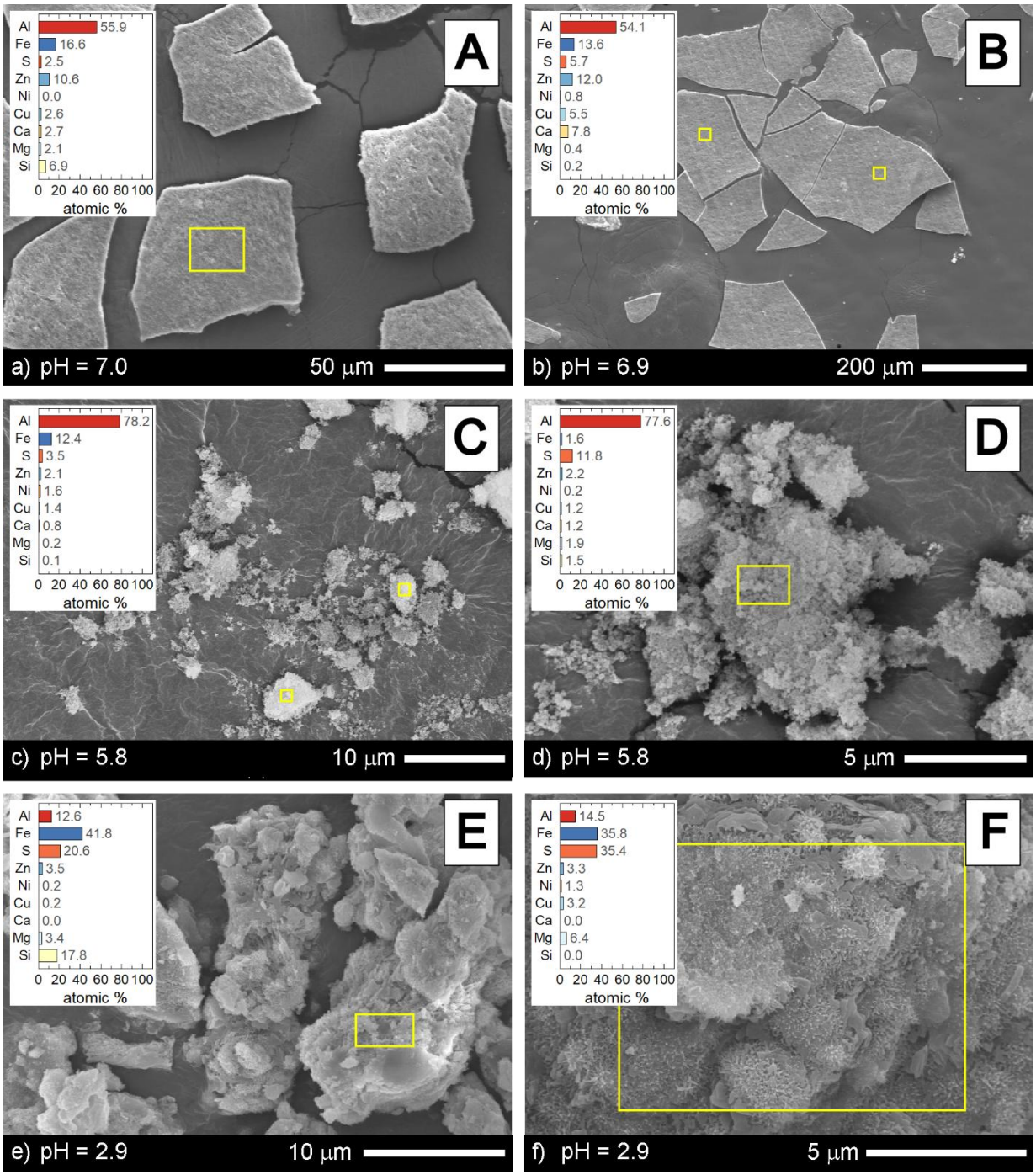

Figure S12. Scanning electron microscope images of suspended particles driving water discoloration downstream of vegetation dieback (KM99 stream, Mackenzie River basin, July 2024). Yellow boxes indicate areas targeted for chemical analyses by electron dispersive spectroscopy.

5

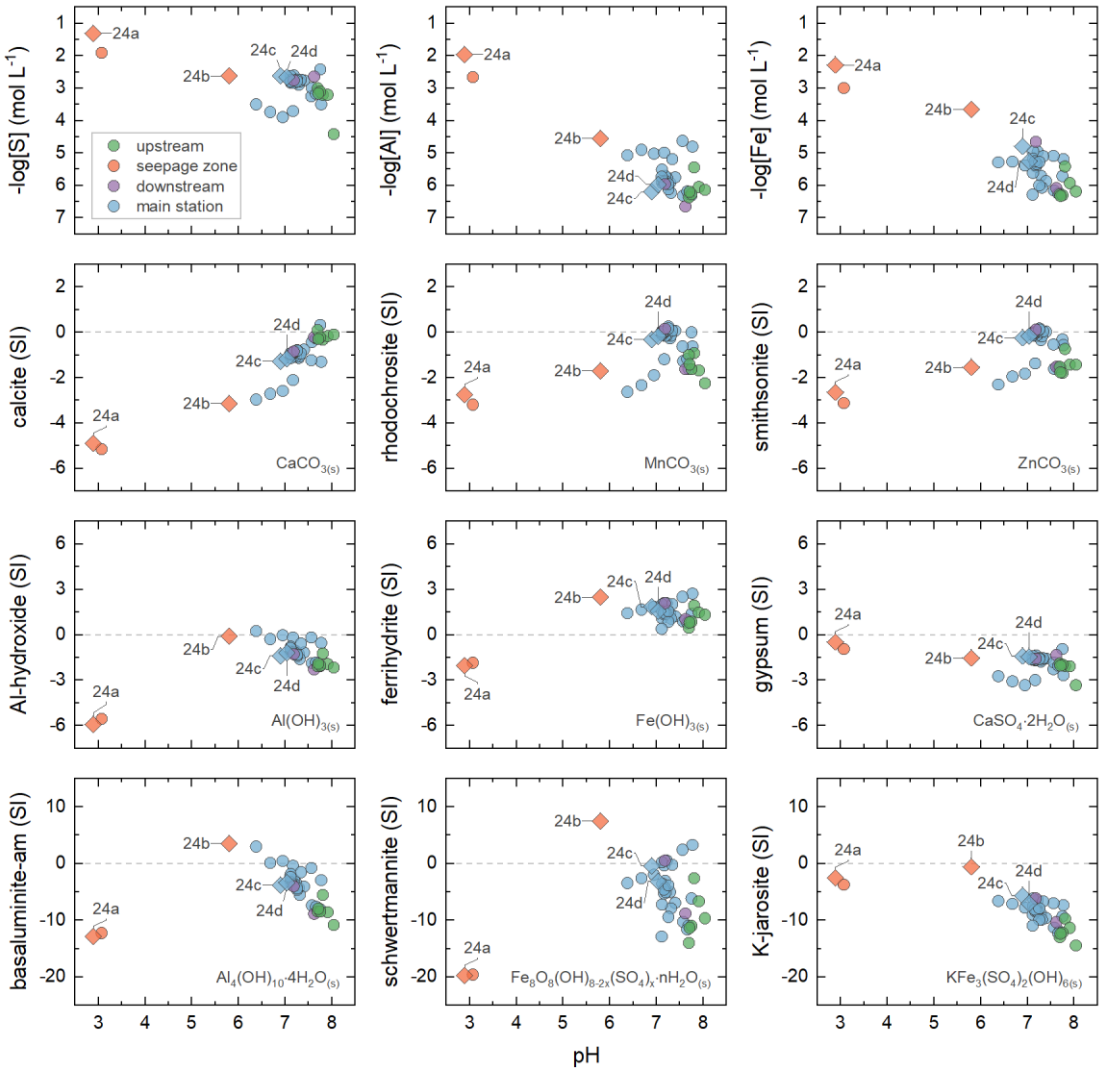

Figure S13. Mineral saturation indices (SI) in a headwater stream receiving acidic seepage in an area of vegetation dieback (KM99 stream, Mackenzie River basin). Symbols are grouped by location relative to acidic seepage zone. The main monitoring station is at the stream outlet, ~3 km downstream of acidic seepage zone.

5

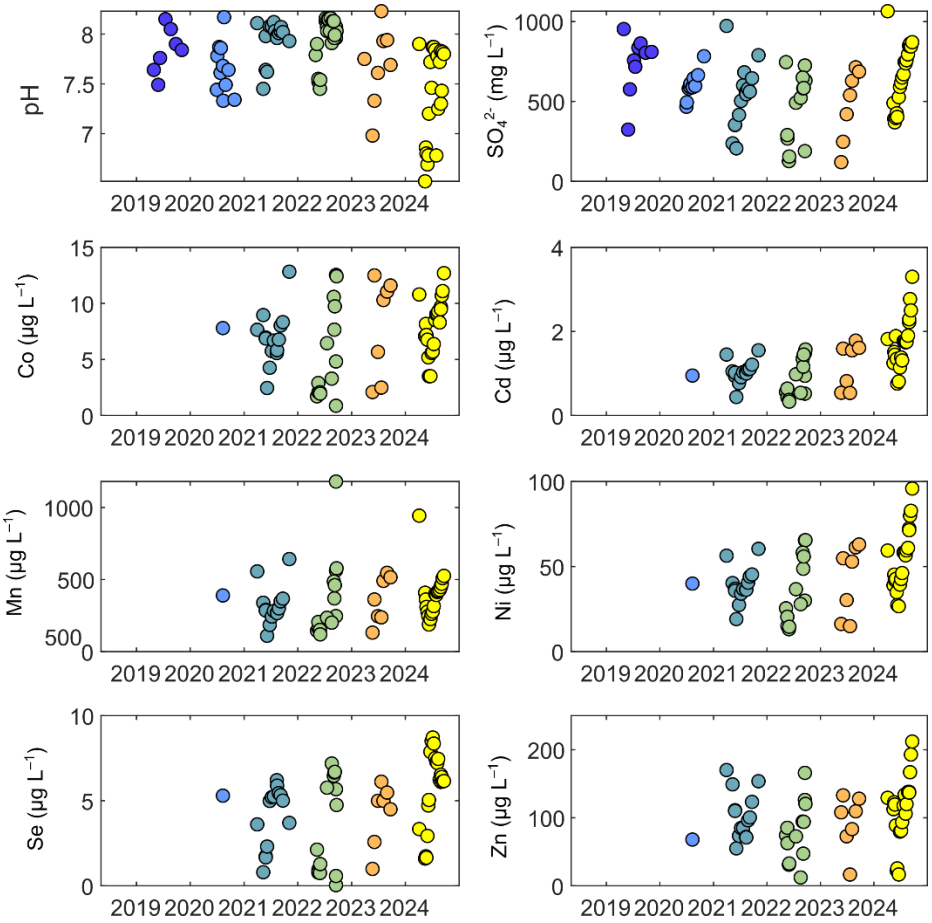

Figure S14. Temporal evolution in pH, sulfate, and metals concentrations in a headwater stream of the Tombstone Waters Observatory (KM71 stream, Yukon River Basin). Symbol colors are grouped by year.

5

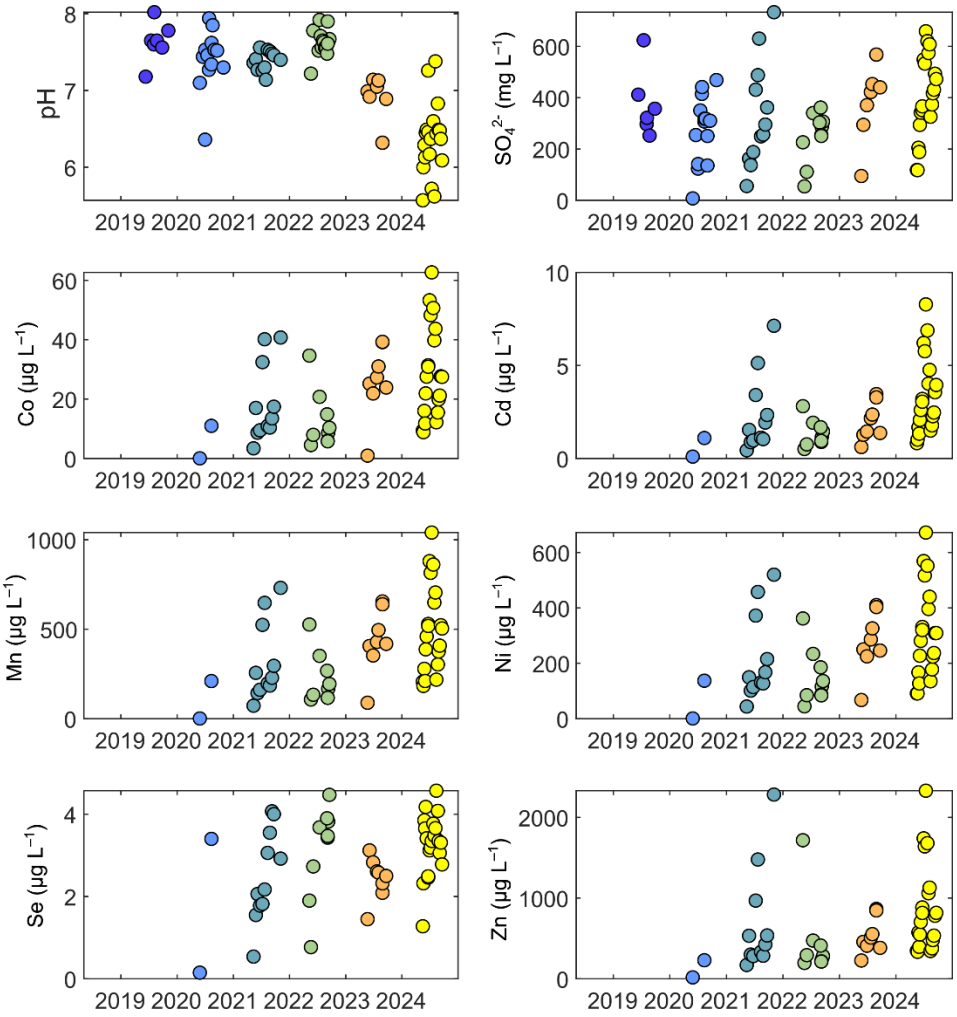

Figure S15. Temporal evolution in pH, sulfate, and metals concentrations in a headwater stream of the Tombstone Waters Observatory (KM175 stream, Mackenzie River Basin). Symbol colors are grouped by year.

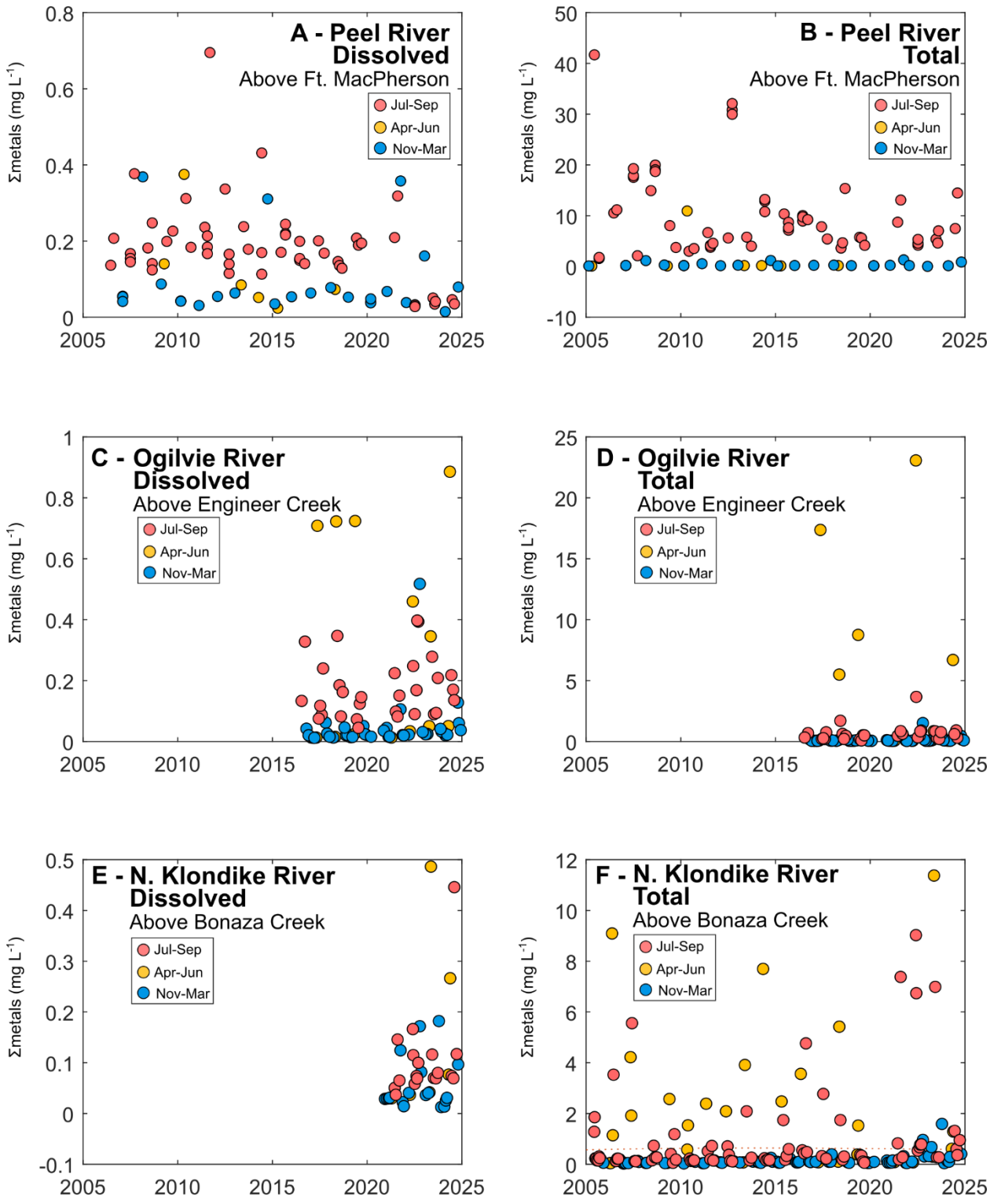

Figure S16. No significant interannual increases in dissolved (A, C, E) and total (B, D, F) metals [Σ(aluminum+iron+manganese+nickel+zinc)] concentrations have occurred in major tributary rivers of the Mackenzie and Yukon rivers downstream of the Tombstone Waters Observatory in recent decades.